

# A preliminary discussion of the real gas effect on the isentropic expansion inlet boundary conditions of high-pressure hydrogen jets

Xinmeng Tang<sup>\*†</sup>, Edyta Dzieminska<sup>\*</sup>, and A. Koichi Hayashi<sup>\*\*</sup>

<sup>\*</sup>Department of Engineering and Applied Sciences, Faculty of Science and Technology, Sophia University, Yotsuya Campus 7-1 Kioi-cho, Chiyoda-ku, Tokyo, 102-8554 JAPAN  
Phone: +81 070-4494-9911

<sup>†</sup>Corresponding author: simondonxq@gmail.com, shimon@pku.edu.cn

<sup>\*\*</sup>Department of Mechanical Engineering, Aoyama Gakuin University, 4-4-25 Shibuya, Shibuya-ku, Tokyo, 150-8366 JAPAN

Received: April 10, 2018 Accepted: July 3, 2019

## Abstract

In some numerical and practical situations, the nozzle inlet boundary quantities  $p_{in}$ ,  $T_{in}$ ,  $\rho_{in}$ , and  $w_{in}$  (the pressure, temperature, density, and axial velocity at the nozzle inlet) are utilized to define the jet flow instead of the stagnation quantities  $p_s$ ,  $T_s$ , and  $\rho_s$  (the stagnation pressure, temperature, and density). In this short note, for given stagnation quantities  $p_s$ ,  $T_s$ , and  $\rho_s$ , the inlet boundary conditions  $p_{in}$ ,  $T_{in}$ ,  $\rho_{in}$ , and  $w_{in}$  are algebraically represented based on a local sonic assumption together with the isentropic expansion and adiabatic flow assumptions by employing three different gas models: the ideal gas model, the Abel-Noble gas model, and the Soave-Redlich-Kwong (SRK) real gas model. It is found that when the ideal gas model is employed, the deviation of inlet boundary condition defined by  $p_{in}$ ,  $T_{in}$ ,  $\rho_{in}$ , and  $w_{in}$  from the real ones (taking the data from the SRK real gas model as reference) due to the real gas effect is much smaller than the deviation of the stagnation quantity  $\rho_s$ . As to the Abel-Noble gas model, though its  $\rho_s$  plot performs well and is quite accurate compared with the referenced SRK real gas model, its deviation of the inlet boundary conditions  $p_{in}$ ,  $T_{in}$ ,  $\rho_{in}$ , and  $w_{in}$  due to the real gas effect is much larger than its deviation of the stagnation quantity  $\rho_s$ . The Abel-Noble gas model is not so ideal to be employed in the hydrogen jet simulation when the nozzle inlet boundary conditions  $p_{in}$ ,  $T_{in}$ ,  $\rho_{in}$ , and  $w_{in}$  are utilized. By these discussion it is made clear that how much the deviation is when for a hydrogen jet calculation the ideal gas or Abel-Noble gas model is utilized to determine the nozzle inlet boundary conditions  $p_{in}$ ,  $T_{in}$ ,  $\rho_{in}$ , and  $w_{in}$ .

**Keywords:** high pressure, hydrogen jet, inlet boundary condition, nozzle inlet, real gas effect

## 1. Introduction

Hydrogen has some unique characteristics that make it an ideal energy carrier<sup>1)</sup> like high conversation efficiency with electricity, cleanness and good environmental compatibility. The transition to a hydrogen economy may have already begun in the recent decade<sup>2)</sup>. At present, there are a large number of companies and national projects in Europe, Japan, Canada, the United States, Korea, and China working on technologies pertaining to hydrogen production, storage, and utilization. Meanwhile, due to its extremely low ignition energy and a wide range

of flammability limits, hydrogen has a reputation for spontaneous ignition, making its utilization more dangerous than that of other fuels. In addition, hydrogen's high diffusion property and high burning velocity intensify the challenge of its safe usage.

One of the technologies for hydrogen storage is the above ground pressurized hydrogen storage system. Usually, it is of very high pressures for both volumetric and gravimetric efficiencies. In this case, the hazards associated with accidental leakage must be considered. The hydrogen jet from such leaks needs to be critically

evaluated and discussed to make sure that its resultant hydrogen cloud is safely and critically controlled to prevent the potential hazard and quantify the risk. In the last decade, a large number of numerical works have been conducted to investigate hydrogen jets assuming that unintended releases of hydrogen occur with various gas models.

Among these works, the Beattie-Bridgeman real gas equation of state (EOS) was employed by Mohamed et al.<sup>3)</sup> in the adiabatic release of hydrogen from a high-pressure chamber. The Abel-Nobel EOS was referred in work by Schefer et al.<sup>4)</sup> which discussed the characterization of high-pressure, underexpanded hydrogen-jet flames. This real gas model was also discussed in works by Tchouvelev et al.<sup>5)</sup>. Both the Beattie-Bridgeman and Abel-Nobel EOS were employed by Khaksarfard et al.<sup>6).7)</sup> to high-pressure hydrogen jets with a stagnation pressure  $p_s$  up to 70 MPa. The reservoir is included in the numerical mesh so the stagnation pressure  $p_s$ , temperature  $T_s$ , and density  $\rho_s$  could be used to define the hydrogen jet. High-pressure hydrogen gas flows were simulated by Kim et al.<sup>8)</sup> with both the ideal gas and the Redlich-Kwong (RK) gas EOSs. A noticeable difference was reported when the pressure was high. Xiao et al.<sup>9)</sup> presented models based on an isentropic expansion model with a real gas EOS called modern EOS which used the Helmholtz energy as the fundamental property to predict the hydrogen concentration and velocity field in the vicinity of a postulated small leak. Predictions were made for the blow-down of hydrogen reservoirs with the initial pressure of 10, 30 and 100 MPa. The real gas assumption was also introduced into the numerical calculation by Bonelli et al.<sup>10)</sup> when they simulated hydrogen jets from a tank with a stagnation pressure  $p_s$  equal to 75 MPa into still nitrogen at a pressure equal to 5 MPa. Both van der Waals and RK EOSs were implemented. The nozzle inlet boundary conditions  $p_{in}$ ,  $T_{in}$ ,  $\rho_{in}$ , and inlet velocity  $w_{in}$  were utilized to define the jet flows. It was found that the results are strongly affected by the EOS. In work by Li et al.<sup>11)</sup> they utilized Soave-Redlich-Kwong (SRK) real gas EOS for the near-field region and the ideal gas EOS for far-field gas properties to simulate a pressurized hydrogen jet with a stagnation pressure  $p_s$  of 20 MPa and achieved a good agreement with experimental data.

Meanwhile, the ideal gas EOS is still widely utilized in many works about hydrogen jets/release. Makarov et al.<sup>12)</sup> presented results of numerical simulations of hydrogen highly under-expanded jets from a storage vessel at pressure 40 MPa through a circular nozzle and two plane nozzles with aspect ratios 5.0 and 12.8 which used the ideal gas model. It was reported that the simulations were in good agreement with experimental data. Under-expanded hydrogen jets with nozzle pressure ratios (NPR) of 8.5, 10, 30 and 70 were simulated in a large eddy simulation (LES) work and compared with methane jets by Hamzehloo et al.<sup>13).14)</sup>. A Reynolds-averaged Navier-Stokes (RANS) simulation was performed by Tsuboi et al.<sup>15)</sup> on hydrogen jet with a pressure of 82 MPa and  $d=0.2$  mm.

In our previous works<sup>16).17)</sup>, we have numerically investigated the three-dimensional (3D) hydrogen jet with a storage pressure of 82 MPa and a tiny jet orifice diameter of 0.2 mm by the full compressible Navier-Stokes equations together with the ideal gas assumption. An adaptive mesh refinement (AMR) technology was assembled to reduce the number of grid cells. Firstly, the starting transient evolution and Mach disk stabilization were discussed in details. Later, both the instantaneous and mean hydrogen concentration distributions in the free hydrogen jet were discussed. On one hand, it is known that the ideal gas model would lead to a large deviation on the stagnation density  $\rho_s$ . For the case with a  $p_s$  of 82 MPa, the deviation percentage is as large as 55%. If this deviation is introduced into the computational simulation, then the results are supposed to end up with too much distortion and be unacceptable. On the other hand, though the ideal gas equation was employed, the calculated hydrogen profile under such high stagnation pressure characterized by the time-averaged hydrogen concentration  $\bar{C}_{H_2}$  turned out to roughly agree with the experimental results. These two aspects above suggest that for the jet simulation employing the ideal gas equation its deviation from the accurate solution would be overestimated if the evaluation is operated from the perspective of the stagnation density's deviation which is very large. During the usage of the ideal gas model, why is the deviation of simulation results not as large as the deviation of stagnation density  $\rho_s$  suggests? Why can the ideal gas still roughly work at such a high pressure as 82 MPa?

In these simulations<sup>16).17)</sup> it is not the stagnation quantities  $p_s$ ,  $T_s$  and  $\rho_s$  but the nozzle inlet boundary conditions  $p_{in}$ ,  $T_{in}$ ,  $\rho_{in}$ , and  $w_{in}$  (the pressure, temperature, density, and axial velocity at the nozzle inlet) that directly defines the jet flow. Here the subscript "in" represents the nozzle inlet. These  $p_{in}$ ,  $T_{in}$ ,  $\rho_{in}$ , and  $w_{in}$  were calculated from the stagnation quantities  $p_s$ ,  $T_s$ , and  $\rho_s$  based on a local sonic assumption together with the isentropic expansion relation and the enthalpy relation. Therefore, to answer the above questions, it is essential to understand how the real gas effect reflects on the nozzle inlet boundary conditions  $p_{in}$ ,  $T_{in}$ ,  $\rho_{in}$ , and  $w_{in}$ .

In this paper, the inlet boundary conditions  $p_{in}$ ,  $T_{in}$ ,  $\rho_{in}$ , and  $w_{in}$  are algebraically represented based on three gas models: the ideal gas model, the Abel-Noble gas model, and the SRK real gas model. The physical relations are given based on a local sonic assumption together with the isentropic expansion relation and the enthalpy relation. By doing this the deviation of inlet boundary conditions can be evaluated.

Hence this paper is generally organized as follows: firstly a brief introduction is given about the investigations of hydrogen jets of various stagnation quantities  $p_s$ ,  $T_s$ , and  $\rho_s$ . In the second section, the calculation modeling and frameworks will be represented including the brief physical problem and physical relations of inlet boundary conditions  $p_{in}$ ,  $T_{in}$ ,  $\rho_{in}$ , and  $w_{in}$  at the jet nozzle. Finally, based on these frameworks the real gas effect reflects on

the inlet boundary conditions  $p_{in}$ ,  $T_{in}$ ,  $\rho_{in}$ , and  $w_{in}$  will be discussed for given stagnation pressures  $p_s$  in the range of 0.1 MPa to 140 MPa and a fixed temperature  $T_s$  of 300 K. Lastly, the conclusion will be drawn based on the discussion.

## 2. Calculation modeling and frameworks

### 2.1 Physical problem model

The physical problem in this work is the pressurized hydrogen injected into an open space as shown in Figure 1. The stagnation temperature  $T_s$  is kept at 300 K while its stagnation pressure  $p_s$  is discussed in the range of 0.1 MPa to 140 MPa.

### 2.2 Physical relations of inlet boundary conditions at the nozzle

No nozzle shape is specified. At the nozzle position, the inlet boundary condition can be given by a local sonic assumption together with isentropic expansion laws and an assumption of an adiabatic flow. Sometimes in the below discussion, the injection speed may be set to be subsonic for comparison. Then the physical relations

$$ds = 0 \quad (1)$$

and

$$h_s + \frac{1}{2}w_s^2 = h_{in} + \frac{1}{2}w_{in}^2 \quad (2)$$

can be obtained. Here  $s$  indicates the specific entropy defined as

$$ds = \frac{c_v}{T}dT + \left(\frac{\partial p}{\partial T}\right)_v dv = \frac{c_p}{T}dT - \left(\frac{\partial v}{\partial T}\right)_p dp \quad (3)$$

$w$  is the velocity component in the axial direction.  $w_s$  is zero while  $w_{in}$  is equal to a certain  $c_{in}$  (dependent on the gas model) due to the local sonic assumption.  $h$  indicates the specific enthalpy which can be given by

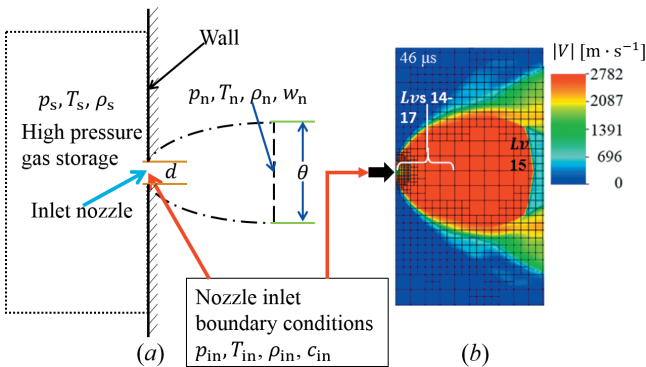


**Figure 1** (a) Schematic of a notional nozzle in an underexpanded jet. Here subscript “s” indicates the storage properties, “n” represents the notional nozzle and subscript “in” indicates the nozzle inlet boundary properties.  $\theta$  is the notional nozzle diameter or effective nozzle diameter and  $d$  is the physical nozzle diameter. (b) a numerical hydrogen jet result adapted from Tang *et al.*<sup>17)</sup> which is defined by the nozzle inlet boundary quantities  $p_{in}$ ,  $T_{in}$ ,  $\rho_{in}$ , and  $c_{in}$  instead of  $p_s$ ,  $T_s$ , and  $\rho_s$ . Near-field velocity magnitude is shown for this hydrogen jet with  $p_s$  of 82 MPa.

$$dh = Tds + vdp = c_p dT + \left[ v - T \left( \frac{\partial v}{\partial T} \right)_p \right] dp \quad (4)$$

and here  $v$  is the specific volume given by density  $\rho$  as

$$v = \frac{1}{\rho} \quad (5)$$

The specific internal energy  $e$  can be expressed as

$$de = Tds - pdv = c_v dT + \left[ T \left( \frac{\partial p}{\partial T} \right)_v - p \right] dv \quad (6)$$

Above  $c_p$  and  $c_v$  indicate the specific heat capacities of gases at constant pressure and that at constant volume, respectively, defined as

$$c_v = \left( \frac{\partial e}{\partial T} \right)_p \quad (7)$$

and

$$c_p = \left( \frac{\partial h}{\partial T} \right)_p = \left( \frac{\partial e}{\partial T} \right)_p + p \left( \frac{\partial v}{\partial T} \right)_p \quad (8)$$

Besides, the general expression of sound speed  $c$  is required which is

$$c^2 = \left( \frac{\partial p}{\partial \rho} \right)_s = \gamma \left( \frac{\partial p}{\partial \rho} \right)_T \quad (9)$$

where  $\gamma$  is the specific heats ratio defined as

$$\gamma = \frac{c_p}{c_v} \quad (10)$$

With the above relations together with the gas equations of state (EOS) specified below, the inlet boundary conditions  $p_{in}$ ,  $T_{in}$ ,  $\rho_{in}$ , and  $w_{in}$  can be algebraically calculated and discussed for evaluating the deviation of inlet boundary conditions due to the real gas effect and for the subsequent numerical simulation which would assemble the real gas model.

### 2.3 Nozzle inlet boundary conditions $p_{in}$ , $T_{in}$ , $\rho_{in}$ , and $w_{in}$

#### 2.3.1 Ideal gas model

For the calorically perfect gas, its  $p$ - $v$ - $T$  relation satisfies the ideal gas EOS as

$$p = \rho RT = \rho \frac{\mathcal{R}}{W} T \quad (11)$$

Here  $R$  is the gas constant for a specified gas,  $\mathcal{R}$  is the universal gas constant as  $8.3143 \text{ J}\cdot\text{mol}^{-1}\cdot\text{K}^{-1}$  and  $W$  is the molecular weight of the hydrogen gas.

For the ideal gas  $c_p$  and  $c_v$  only depend on temperature. We use the superscript 0 to identify the physical variables of the ideal gas.  $c_p^0(T)$  and  $c_v^0(T)$  can be given by

$$c_p^0(T) = R (a_1 + a_2 T + a_3 T^2 + a_4 T^3 + a_5 T^4) \quad (12)$$

$$c_v^0(T) = R (a_1 + a_2 T + a_3 T^2 + a_4 T^3 + a_5 T^4) - R \quad (13)$$

where  $a_1, \dots, a_7$  are constants in the standard seven-coefficient polynomials of McBride *et al.*<sup>18)</sup>.  $h$  can be expressed as

$$h^0 = c_p^0 T = \frac{\gamma RT}{\gamma - 1} = \frac{\gamma}{\gamma - 1} \frac{p}{\rho} \quad (14)$$

In the ideal gas the sound speed defined in Equation (9) can be deduced as

$$c = \sqrt{\gamma RT} \quad (15)$$

Then from Equations (2), (14), and (15) we can get the relation

$$\frac{T}{T_s} = \frac{1}{1 + \frac{\gamma - 1}{2} M^2} \quad (16)$$

where  $M$  indicates Mach number.

The isentropic expansion relation about the specific entropy  $s$  can be deduced into

$$\frac{p}{p_s} = \left(\frac{\rho}{\rho_s}\right)^\gamma = \left(\frac{T}{T_s}\right)^{\frac{\gamma}{\gamma - 1}} \quad (17)$$

for the calorically perfect gas.

By Equations (16) and (17) the relations of  $p$  and  $\rho$  for the calorically perfect gas can be simplified as

$$\frac{p_{in}}{p_s} = \left(1 + \frac{\gamma - 1}{2} M^2\right)^{\frac{-\gamma}{\gamma - 1}} \quad (18)$$

and

$$\frac{\rho_{in}}{\rho_s} = \left(1 + \frac{\gamma - 1}{2} M^2\right)^{\frac{-\gamma}{\gamma - 1}} \quad (19)$$

Take  $\gamma$  from Equation (9) as

$$\gamma = \frac{c_p^0(T)}{c_v^0(T)} \quad (20)$$

and let  $M$  to be 1.0, then the inlet physical parameters  $p_{in}$ ,  $T_{in}$ ,  $\rho_{in}$ , and  $w_{in}$  ( $M = 1.0$ ) can be computed from the given  $p_s$  and  $T_s$ .

### 2.3.2 Abel-Noble gas model

One of the simple equations of real gas models is the Abel-Noble EOS which is

$$p = \frac{\rho RT}{1 - b\rho} = Z\rho RT \quad (21)$$

where  $Z = 1/(1 - b\rho) = pv/RT$  is the compressibility factor and  $b$  is the co-volume constant. It is  $7.691 \times 10^{-3} \text{ m}^3 \cdot \text{kg}^{-1}$  for hydrogen. When  $b$  is set to zero it becomes the EOS for an ideal gas.

Based on the Abel-Noble EOS, the isentropic flow relations which are expressed in Equations (16) and (18), (19) for ideal gas above comes to derivatives as<sup>4)</sup>

$$\left(\frac{\rho_s}{1 - b\rho_s}\right)^\gamma = \left(\frac{\rho_{in}}{1 - b\rho_{in}}\right)^\gamma \left[1 + \frac{\gamma - 1}{2(1 - b\rho_{in})} M^2\right]^{\frac{\gamma}{\gamma - 1}} \quad (22)$$

and

$$\frac{T_{in}}{T_s} = \frac{1}{1 + \frac{\gamma - 1}{2(1 - b\rho_{in})^2} M^2} \quad (23)$$

For simplification and accuracy, here  $\gamma$  is valued using

the NIST data at the corresponding  $p_s$  and  $T_s$ . By solving Equation (22) through the Newton-Rapson method with  $M = 1$ , we can get the density at the nozzle inlet  $\rho_{in}$ . Accordingly at the nozzle inlet  $T_{in}$  can be calculated with Equation (23).

Meanwhile, the sound speed  $c$  under Abel-Noble gas EOS evolves into

$$c_{in} = \frac{1}{1 - b\rho_{in}} \sqrt{\gamma RT_{in}} \quad (24)$$

### 2.3.3 SRK real gas model

For the widely used cubic EOS

$$p = \frac{RT}{v - b} - \frac{a}{v^2 + mbv + nb^2} \quad (25)$$

where  $a$  is a function of  $T$  and  $m$  and  $n$  depend on different cubic EOS models. The systematic equations of these thermodynamic quantities including the specific internal energy  $e(T, v)$ , specific enthalpy  $h(T, p)$ , specific entropy  $s(T, p)$ , speed of sound  $c$  together with specific heat capacities  $c_v$  and  $c_p$ , are not at one's fingertips. Here the preliminary frameworks of thermodynamic properties for a real gas are systematically prepared for the below discussion and usage of the following works which contains the real gas effect.

The cubic EOS mainly includes Van der Waal model<sup>19)</sup>, RK model<sup>20)</sup>, SRK model<sup>21)</sup>, Peng-Robinson (PR) model<sup>22)</sup>, and Patel-Teja (PT) model<sup>23)</sup>. For these EOSs the calculations in the previous section become more complicated and Equations (22)–(24) cannot work anymore. We need the fundamental definition equations of these thermodynamic quantities, as listed in Equations (3), (4) and (6) – (10), to get the properties of a real gas.

From these fundamental definition equations, it has the specific internal energy for a real gas as

$$e(T, v) = e^0(T) + \int \left[ T \left( \frac{\partial p}{\partial T} \right)_v - p \right] dv \quad (26)$$

the specific enthalpy as

$$h(T, p) = h^0(T) + \int \left[ v - T \left( \frac{\partial v}{\partial T} \right)_p \right] dp \quad (27)$$

and the specific entropy as

$$s(T, p) = s^0(T, p) - \int \left[ T \left( \frac{\partial v}{\partial T} \right)_p - \frac{R}{p} \right] dp \quad (28)$$

Here

$$e^0(T) = c_v^0(T) T = R \left( a_1 T + \frac{a_2 T^2}{2} + \frac{a_3 T^3}{3} + \frac{a_4 T^4}{4} + \frac{a_5 T^5}{5} + a_6 \right) - RT \quad (29)$$

$$h^0(T) = c_p^0(T) T = R \left( a_1 T + \frac{a_2 T^2}{2} + \frac{a_3 T^3}{3} + \frac{a_4 T^4}{4} + \frac{a_5 T^5}{5} + a_6 \right) \quad (30)$$

and

$$s^0(T, p) = R \left( a_1 \ln T + a_2 T + \frac{a_3 T^2}{2} + \frac{a_4 T^3}{3} + \frac{a_5 T^4}{4} + a_7 \right) - R \ln \frac{p}{p_0} \quad (31)$$

are the specific internal energy, enthalpy and entropy of the corresponding ideal gas, respectively.

The SRK EOS can be expressed as

$$p = \frac{RT}{v-b} - \frac{a}{v^2 + mbv + nb^2} \quad (32)$$

where

$$m = 1, n = 0, \quad (33)$$

$$a \equiv a(T) = 0.42748 \frac{R^2 T_{cr}^2}{p_{cr}} \left[ 1 + f(\omega_a) \left( 1 - \sqrt{\frac{T}{T_{cr}}} \right) \right]^2 \quad (34)$$

$$b = 0.08664 R \frac{T_{cr}}{p_{cr}} \quad (35)$$

and

$$f(\omega_a) = 0.48 + 1.574\omega_a - 0.176\omega_a^2 \quad (36)$$

Here  $\omega_a$  is the acentric factor whilst  $p_{cr}$  and  $T_{cr}$  are the gas's critical pressure and temperature, respectively.  $e(T, v)$  for a real gas can be given based on the SRK EOS as

$$e(T, v) = e^0(T) + \frac{1}{b} \left[ a(T) - T \frac{\partial a(T)}{\partial T} \right] \ln \frac{v}{v+b} \quad (37)$$

where

$$\frac{\partial a(T)}{\partial T} = -0.42748 \frac{R^2 T_{cr}^2}{p_{cr}} f(\omega_a) \left\{ [1 + f(\omega_a)] \sqrt{\frac{1}{T_{cr} T}} - f(\omega_a) \frac{1}{T_{cr}} \right\} \quad (38)$$

Similarly, the specific enthalpy  $h$  for a real gas can be obtained by the ideal  $h^0(T)$  together with its departure function as

$$h(T, v) = h^0(T) + RT \left( \frac{pv}{RT} - 1 \right) + \frac{1}{b} \left[ a(T) - T \frac{\partial a(T)}{\partial T} \right] \ln \frac{v}{v+b} \quad (39)$$

and the specific entropy  $s$  as

$$s = s^0(T, p) + R \ln \frac{p(v-b)}{RT} + \frac{1}{b} \frac{\partial a(T)}{\partial T} \ln \frac{v}{v+b} \quad (40)$$

With these specific internal energy, enthalpy, and entropy calculated, then  $c_v$  in the SRK model can be given as

$$c_v = \left( \frac{\partial e}{\partial T} \right)_\rho = c_v^0(T) - \frac{1}{b} \ln \frac{v}{v+b} \frac{\partial^2 a(T)}{\partial T^2} T \quad (41)$$

where

$$\frac{\partial^2 a(T)}{\partial T^2} = 0.21374 \frac{R^2 T_{cr}^2}{p_{cr}} f(\omega_a) [1 + f(\omega_a)] \sqrt{\frac{1}{T_{cr} T^3}} \quad (42)$$

and  $c_p$  can be calculated from  $c_v$  based on Equations (5)–(8) together with the Maxwell relations as

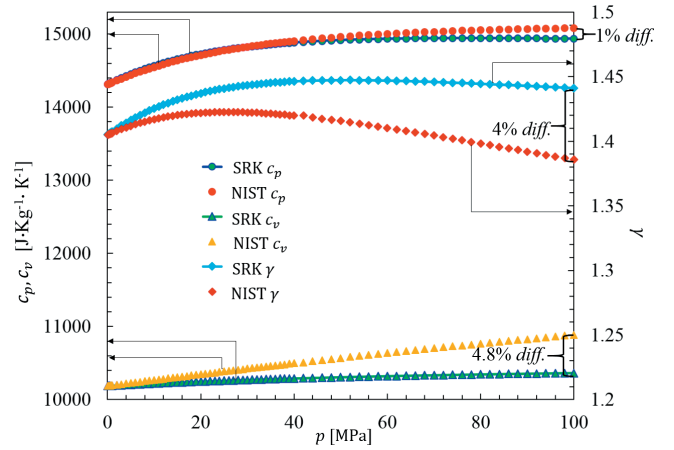


**Figure 2** Specific heat capacities  $c_p$  and  $c_v$  and the specific heat ratio  $\gamma$  given by the SRK gas model, compared with the NIST data in the range of  $p_s \sim [0.1, 100]$  MPa with a fixed temperature  $T_s$  of 300 K. The deviation of  $c_p$  is within 1% while it's 4.8% for  $c_v$  and 4% for  $\gamma$ .

$$c_p = c_v + T \left( \frac{\partial p}{\partial T} \right)_\rho \left( \frac{\partial v}{\partial T} \right)_p = c_v - \frac{T \left( \frac{\partial p}{\partial T} \right)_\rho}{\left( \frac{\partial p}{\partial v} \right)_T}$$

$$= c_v^0(T)$$

$$+ T \left\{ \frac{\left[ \frac{R}{v-b} \frac{\partial a(T)}{\partial T} \right]^2}{\frac{RT}{(v-b)^2} - \frac{a(T)}{(v^2 + bv)^2} (2v+b)} - \frac{1}{b} \ln \frac{v}{v+b} \frac{\partial^2 a(T)}{\partial T^2} \right\} \quad (43)$$

Substituting Equations (41) and (43) into Equation (10) gives

$$\gamma(T, v) = 1 + \frac{T \left[ \frac{R}{v-b} \frac{\partial a(T)}{\partial T} \right]^2}{\left[ \frac{RT}{(v-b)^2} - \frac{a(T)}{(v^2 + bv)^2} (2v+b) \right] \left[ c_v^0(T) - \frac{1}{b} \ln \frac{v}{v+b} \frac{\partial^2 a(T)}{\partial T^2} \right]} \quad (44)$$

The speed of sound in Equation (9) gives

$$c^2 = \frac{\gamma(T, v) RT v^2}{(v-b)^2} - \frac{\gamma(T, v) v^2 a(T)}{(v^2 + bv)^2} (2v+b) \quad (45)$$

Above are the thermodynamical frameworks based on the SRK EOS. A validation is presented by comparing the SRK data against the NIST data in the range of  $p_s \sim [0.1, 100]$  MPa with a fixed temperature  $T_s$  of 300 K, as shown in Figure 2. The deviation of  $c_p$  is within 1% while it's 4.8% for  $c_v$  and 4% for  $\gamma$ . The agreement is quite good.

Under such frameworks, the isentropic relation in Equation (1) and the enthalpy relation in Equation (2) together with the local sonic assumption give the equations

$$f_2(p, T, v) = R \left( a_1 \ln T + a_2 T + \frac{a_3 T^2}{2} + \frac{a_4 T^3}{3} + \frac{a_5 T^4}{4} + a_7 \right) + R \ln \frac{(v-b)p_0}{RT} + \frac{1}{b} \frac{\partial a(T)}{\partial T} \ln \frac{v}{v+b} - s_s(p_s, T_s, v_s) = 0 \quad (46)$$

and

$$f_3(p, T, v) = R \left( a_1 T + \frac{a_2 T^2}{2} + \frac{a_3 T^3}{3} + \frac{a_4 T^4}{4} + \frac{a_5 T^5}{5} + a_6 \right) + pv - RT + \frac{1}{b} \left[ a(T) - T \frac{\partial a(T)}{\partial T} \right] \ln \frac{v}{v+b} + \frac{\gamma(T, v) RT v^2}{2(v-b)^2} - \frac{\gamma(T, v) v^2 a(T)}{2(v^2 + bv)^2} (2v+b) - h_s(p_s, T_s, v_s) = 0 \quad (47)$$

These equations form a nonlinear system of equations  $\mathbf{F}$  as

$$\mathbf{F} = \begin{bmatrix} SRK(p, T, v) \\ s_{in}(p, T, v) - s_s(p_s, T_s, v_s) \\ h_{in}(p, T, v) + \frac{1}{2} w(p, T, v)^2 - h_s(p_s, T_s, v_s) \end{bmatrix} = \begin{bmatrix} f_1(p, T, v) \\ f_2(p, T, v) \\ f_3(p, T, v) \end{bmatrix} = \mathbf{0} \quad (48)$$

where the unknown quantities vector is

$$\mathbf{x} \equiv (p_{in}, T_{in}, v_{in})^T \quad (49)$$

Here the first function is given by the SRK equation in Equations (32)–(36) as

$$f_1(p, T, v) = \frac{RT}{v-b} - \frac{a(T)}{v^2 + bv} - p \quad (50)$$

By this nonlinear system of equations the nozzle boundary conditions  $p_{in}$ ,  $T_{in}$ ,  $\rho_{in}$ , and  $w_{in}$  at the nozzle inlet can be obtained from arbitrary given stagnation pressure  $p_s$  and temperature  $T_s$  (then  $v_s$ ). Such a nonlinear system of equations can be solved by the Newton-Rapson method as

$$\mathbf{F}' \equiv \frac{\partial \mathbf{F}}{\partial \mathbf{x}} = \begin{bmatrix} \frac{\partial f_1(p, T, v)}{\partial p} & \frac{\partial f_1(p, T, v)}{\partial T} & \frac{\partial f_1(p, T, v)}{\partial v} \\ \frac{\partial f_2(p, T, v)}{\partial p} & \frac{\partial f_2(p, T, v)}{\partial T} & \frac{\partial f_2(p, T, v)}{\partial v} \\ \frac{\partial f_3(p, T, v)}{\partial p} & \frac{\partial f_3(p, T, v)}{\partial T} & \frac{\partial f_3(p, T, v)}{\partial v} \end{bmatrix} \quad (51)$$

and

$$\begin{pmatrix} p \\ T \\ v \end{pmatrix}^{n+1} = \begin{pmatrix} p \\ T \\ v \end{pmatrix}^n - (\mathbf{F}')^{-1} \begin{bmatrix} f_1(p, T, v) \\ f_2(p, T, v) \\ f_3(p, T, v) \end{bmatrix}^n \quad (52)$$

Then within less than five iterations the inlet boundary conditions  $p_{in}$ ,  $T_{in}$ ,  $\rho_{in}$ , and  $w_{in}$  can be obtained.

### 3. Comparison and discussion

Three gas models above, which are the ideal gas model, the Abel-Noble gas model, and the SRK real gas model, are represented together with the calculation frameworks to solve the nozzle inlet boundary conditions  $p_{in}$ ,  $T_{in}$ ,  $\rho_{in}$  and  $w_{in}$  at the jet nozzle from arbitrary given stagnation pressure  $p_s$  and temperature  $T_s$ . In this process the

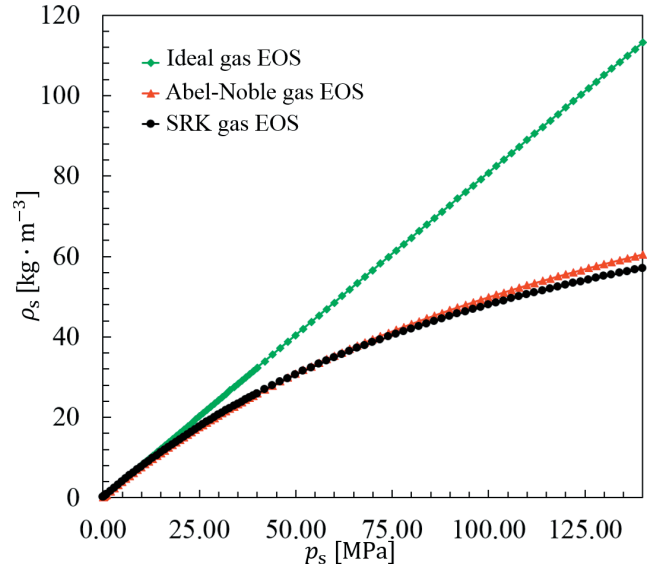


**Figure 3** Relations of stagnation density  $\rho_s$  and stagnation pressure  $p_s$  based on the ideal, Abel-Noble, and SRK gas EOSs in the range of  $p_s \sim [0.1, 140]$  MPa with a fixed temperature  $T_s$  of 300 K.

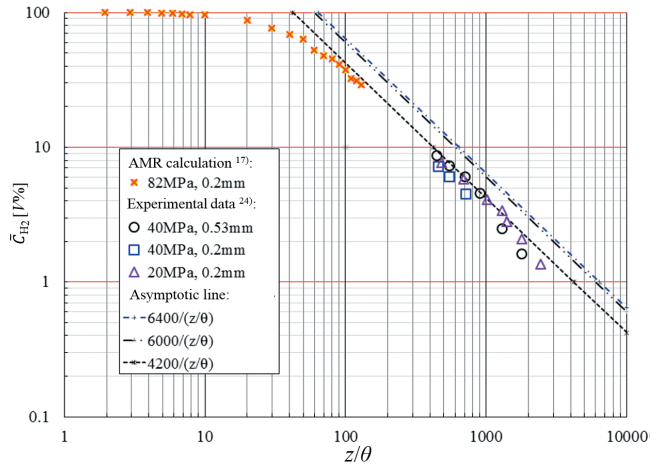


**Figure 4** The previously reported time-averaged axial  $H_2$  concentration of 82 MPa hydrogen jet by 3D computational simulation with the ideal gas assumption<sup>17)</sup>. AMR results are compared with experimental results adapted from Takeno et al.<sup>24)</sup> Here  $\theta$  indicates the effective ejection diameter and  $z$  is the axial distance.

stagnation density  $\rho_s$  is obtained first based on the corresponding EOS which is demonstrated in Figure 3 for given stagnation pressures  $p_s$  in the range of 0.1–140 MPa and a fixed temperature  $T_s$  of 300 K. It can be found that when  $p_s$  is not high, these three EOSs provide very similar  $\rho_s$ , which suggests that the real gas effect is very small. In fact, at the pressures up to about 17.2 MPa, the gas can be treated to a good approximation as ideal. When  $p_s$  gets higher, the ideal EOS cannot work very well and its deviation gets more significant. As mentioned above, when  $p_s$  is 82 MPa this deviation percentage is as large as 55%, as represented in Table 1.

However, although the ideal gas equation was employed in the previous simulations<sup>16),17)</sup>, the calculated averaged hydrogen concentration  $\bar{C}_{H_2}$  with a  $p_s$  of 82 MPa turned out to roughly agree with the experimental results, as shown

**Table 1** Nozzle exit conditions of hydrogen jet with a stagnation pressure of 82 MPa according to the ideal gas model, Abel-Noble gas model, and SRK gas model. Besides, two more SRK cases which assemble the nozzle sound speeds  $c_{in}$  of the ideal gas model or the Abel-Noble gas model are also represented.

	Ideal gas	SRK real gas with ideal nozzle $c_{in}$	Abel-Noble real gas	SRK real gas with Abel-Noble nozzle $c_{in}$	SRK real gas
$p_s$ [MPa]	82.0	82.0	82.0	82.0	82.0
$T_s$ [K]	300.0	300.0	300.0	300.0	300.0
$\rho_s$ [ $\text{kg}\cdot\text{m}^{-3}$ ]	66.273	42.656	43.898	42.656	42.656
$p_{in}$ [MPa]	43.252	53.465	31.42	42.15	36.633
$T_{in}$ [K]	249.494	265.975	228.427	248.567	238.762
$\rho_{in}$ [ $\text{kg}\cdot\text{m}^{-3}$ ]	42.033	35.178	26.543	31.334	29.19
$M_{in}$	1.0	<1.0	1.0	<1.0	1.0
$w_{in}$ [ $\text{m}\cdot\text{s}^{-1}$ ]	1202.34	1202.34	1454.46	1454.46	1572.86

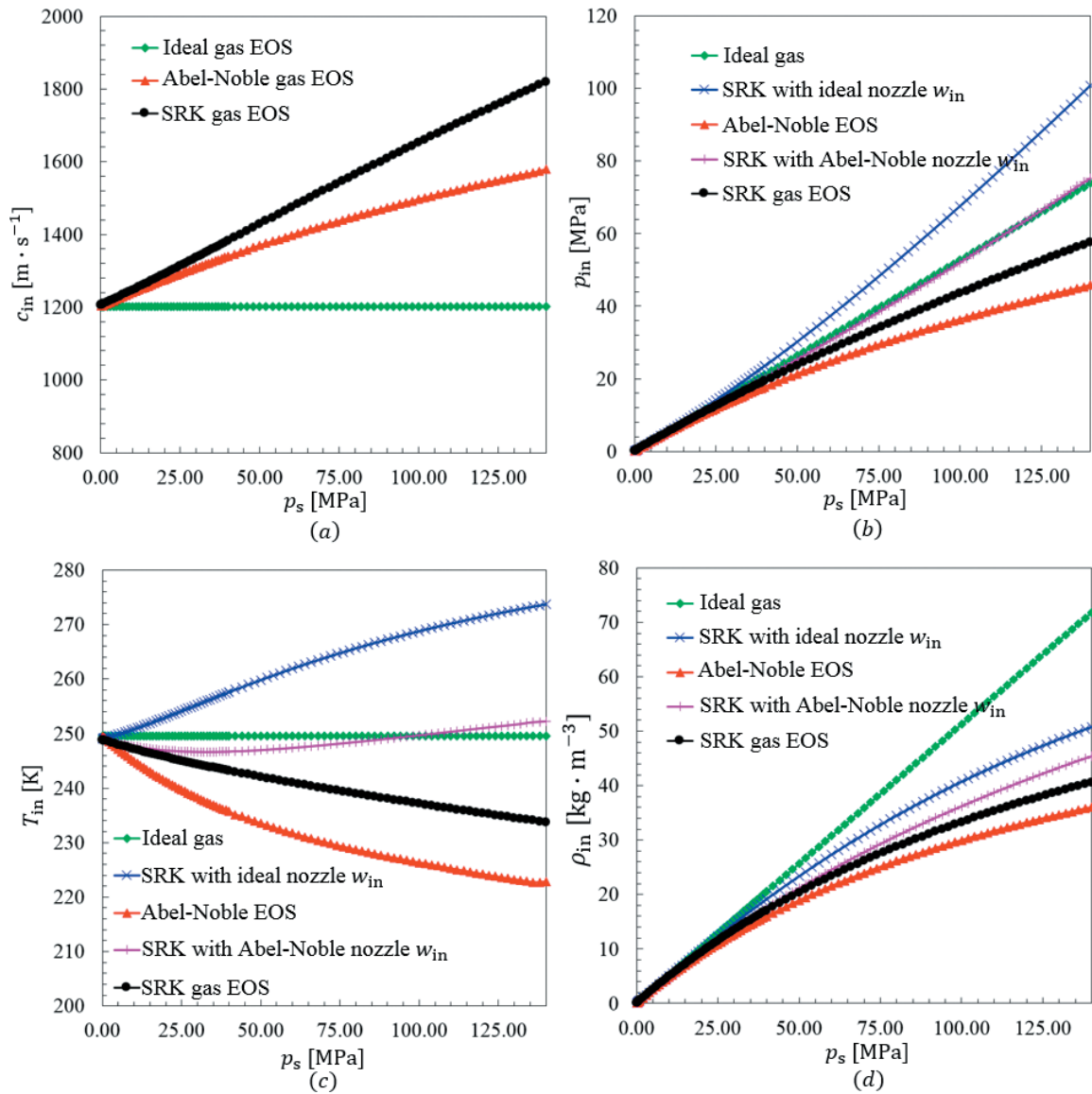


**Figure 5** Inlet nozzle boundary conditions  $p_{in}$ ,  $T_{in}$ ,  $\rho_{in}$ , and  $w_{in}$  based on the ideal gas model, the Abel-Noble gas model, and the SRK real gas model. Besides, two more SRK cases which assemble the nozzle sound speeds  $c_{in}$  of the ideal gas model or the Abel-Noble gas model are also represented.

in Figure 4. These aspects above suggest that for the jet simulation which employs the ideal gas equation its deviation from the accurate solution would be overestimated if the evaluation is operated from the perspective of the stagnation density's deviation which is very large. Why is the deviation of simulation with the ideal gas model not as large as the deviation of stagnation density  $\rho_s$  suggests? Why can the ideal gas still roughly work at such a high pressure?

To answer the above questions, it is essential to understand how the real gas effect reflects on the inlet boundary conditions  $p_{in}$ ,  $T_{in}$ ,  $\rho_{in}$ , and  $w_{in}$ .

Figure 5 illustrates the inlet boundary conditions  $p_{in}$ ,  $T_{in}$ ,  $\rho_{in}$ , and  $w_{in}$  based on the ideal gas model, the Abel-Noble gas model, and the SRK real gas model. Since above we have validated the thermodynamical data from SRK EOS, as illustrated in Figure 2, we here set the results of SRK real gas model illustrated by the black lines in Figure 5 as the reference to discuss the ideal gas model and the Abel-Noble gas model's behaviors. In the ideal gas model the  $c_{in}$  ( $w_{in}=c_{in}$ ) is constant and it is increasingly smaller than the referenced  $c_{in}$  as  $p_{in}$  gets larger. On the contrary,  $p_{in}$ ,  $T_{in}$ , and  $\rho_{in}$  are increasingly larger than these referenced ones. For the  $p_s$  of 82 MPa whose results are listed in Table 1, the  $c_{in}$  based on the ideal gas model is lower than the result of SRK model by 23.56%,  $p_{in}$  is higher by 18.07%,  $T_{in}$  is higher by 4.5%, and  $\rho_{in}$  is higher by 44.0%. Since the ideal gas model's  $c_{in}$  is smaller than the referenced SRK  $c_{in}$ , the inlet boundary conditions  $p_{in}$ ,  $T_{in}$ ,  $\rho_{in}$ , and  $w_{in}$  based on the ideal gas model can be corresponded to a subsonic state in the SRK gas model calculation framework.

By modifying the  $w_{in}$  in Equation (48) by  $c_{in}$  based on the ideal gas model, we can get another SRK inlet boundary conditions  $p_{in}$ ,  $T_{in}$ ,  $\rho_{in}$ , and  $w_{in}$  with which the  $p_{in}$ ,  $T_{in}$ ,  $\rho_{in}$ , and  $w_{in}$  based on the ideal gas model can be compared. These new SRK inlet boundary conditions with the ideal nozzle  $c_{in}$  are plotted in Figure 5 in blue lines. Take them as references and a new group of deviations can be obtained. This time two  $w_{in}$  are the same while for the ideal gas model  $p_{in}$  is lower by 19.1%,  $T_{in}$  is lower by 6.2%, and  $\rho_{in}$  is higher by 19.5% (comparison between the green and blue lines in Figure 5). This group of deviation percentages demonstrates how big the real gas effect on the inlet boundary conditions is in this high-pressure hydrogen jet. It can be seen that these deviations or their integration deviation are much smaller than 55% which is the stagnation density's deviation when  $p_s$  is 82 MPa. It suggests that when the ideal gas model is employed, the deviation of inlet boundary conditions  $p_{in}$ ,  $T_{in}$ ,  $\rho_{in}$ , and  $c_{in}$  due to the real gas effect is smaller than the deviation of stagnation quantities. This explains why the ideal gas can still roughly work at such a high pressure and why the deviation of simulation results is not as large as the deviation of stagnation density  $\rho_s$  suggests since in these simulations<sup>16),17)</sup> it is not the stagnation quantities  $p_s$ ,  $T_s$  and  $\rho_s$  but the nozzle boundary conditions  $p_{in}$ ,  $T_{in}$ ,  $\rho_{in}$ , and  $c_{in}$  that directly define the jet boundary condition at the nozzle exit.

In spite of that the deviation of inlet boundary

conditions  $p_{in}$ ,  $T_{in}$ ,  $\rho_{in}$ , and  $w_{in}$  due to the real gas effect is smaller than the deviation of stagnation quantities when the ideal gas model is employed, it is still significant as discussed above. Therefore, although the ideal gas can still roughly work, it is always recommended that it should be replaced with some real gas model.

As to the Abel-Noble gas model, its  $\rho_s$  plot performs well and is very similar to the SRK result, as shown in Figure 3. However, the deviations of  $p_{in}$ ,  $T_{in}$ ,  $\rho_{in}$ , and  $w_{in}$  from the referenced SRK ones are very significant. They are much larger than the deviation of stagnation quantities, as shown in Figure 5. It is demonstrated that in the perspective of the nozzle inlet boundary conditions  $p_{in}$ ,  $T_{in}$ ,  $\rho_{in}$ , and  $w_{in}$ , the Abel-Noble gas model framework expressed in Equations (21)–(24) does not behave well. For the  $p_s$  of 82 MPa,  $c_{in}$  of the Abel-Noble gas model is lower than the result of the SRK model by 7.53%,  $p_{in}$  is lower by 14.23%,  $T_{in}$  is lower by 4.33% and  $\rho_{in}$  is lower by 9.07%. Similarly as above, since Abel-Noble gas model's  $c_{in}$  is smaller than the referenced SRK  $c_{in}$ , the inlet boundary conditions  $p_{in}$ ,  $T_{in}$ ,  $\rho_{in}$ , and  $w_{in}$  based on the Abel-Noble gas model can be corresponded to a subsonic state in the SRK gas model calculation framework. By modifying the  $c_{in}$  in Equation (48) in to  $c_{in}$  based on the Abel-Noble gas model, we can get another SRK inlet boundary conditions  $p_{in}$ ,  $T_{in}$ ,  $\rho_{in}$ , and  $w_{in}$  with which the  $p_{in}$ ,  $T_{in}$ ,  $\rho_{in}$ , and  $w_{in}$  based on the Abel-Noble gas model can be compared. These new SRK inlet boundary conditions with the Abel-Noble gas model's nozzle  $c_{in}$  are plotted in Figure 5 in pink lines. Taking them as the reference, a new deviation group can be obtained. Now  $c_{in}$  is the same while  $p_{in}$  of the Abel-Noble gas model is lower by 25.46%,  $T_{in}$  is lower by 8.1%, and  $\rho_{in}$  is lower by 15.29% (comparison between the red and pink lines in Figure 5). This group of deviation percentages demonstrates how big the real gas effect on the inlet boundary conditions is in the high-pressure hydrogen jet based on the Abel-Noble gas model. These values based on the Abel-Noble gas model framework are really not positive. All  $p_{in}$ ,  $T_{in}$ , and  $\rho_{in}$  tend to be smaller than the SRK ones. In this aspect, the Abel-Noble gas model framework expressed in Equations (21)–(24) is not so ideal to be employed in the hydrogen jet simulation. Interestingly, the above conclusion is only appropriate when the nozzle inlet boundary conditions  $p_{in}$ ,  $T_{in}$ ,  $\rho_{in}$ , and  $w_{in}$  are employed. If the  $p_s$ ,  $T_s$  and  $\rho_s$  instead of the  $p_{in}$ ,  $T_{in}$ ,  $\rho_{in}$ , and  $w_{in}$  are utilized to determine the hydrogen jet when the tank is included in the calculation, the Abel-Noble gas model would perform pretty well, as reported by Khaksarfard et al.<sup>6)</sup>

#### 4. Conclusions

In this paper the nozzle inlet boundary conditions  $p_{in}$ ,  $T_{in}$ ,  $\rho_{in}$ , and  $w_{in}$  are algebraically represented based on a local sonic assumption together with isentropic expansion laws and an assumption of an adiabatic flow at the jet nozzle by employing three different gas models: the ideal gas model, the Abel-Noble gas model, and the SRK real gas model. It is somehow surprising that the correlation between the deviation of stagnation quantity  $\rho_s$  and the

deviation of  $p_{in}$ ,  $T_{in}$ ,  $\rho_{in}$ , and  $w_{in}$  is so low. Large deviation of stagnation quantity  $\rho_s$  and moderate deviation  $p_{in}$ ,  $T_{in}$ ,  $\rho_{in}$ , and  $w_{in}$  exists in the ideal gas model framework while for the Abel-Noble gas there exists a small deviation of stagnation quantity  $\rho_s$  and moderate deviation of  $p_{in}$ ,  $T_{in}$ ,  $\rho_{in}$ , and  $w_{in}$ . Brief conclusions could be drawn as below:

- (1) When the ideal gas model is employed, the deviation of inlet boundary conditions  $p_{in}$ ,  $T_{in}$ ,  $\rho_{in}$ , and  $w_{in}$  due to the real gas effect is smaller than the deviation of stagnation quantities. For a hydrogen jet with a  $p_s$  of 82 MPa and  $T_s$  of 300 K, the  $\rho_s$  has a deviation as much as 55%. However, compared with the nozzle inlet boundary conditions based on the SRK real gas model with the ideal nozzle  $c_{in}$ ,  $w_{in}$  are the same, while with the ideal gas model  $p_{in}$  is lower by 19.1%,  $T_{in}$  is lower by 6.2%, and  $\rho_{in}$  is higher by 19.5% (comparison between the green and blue lines in Figure 5). This group of deviation is much smaller. This explains why the ideal gas can still roughly work at such a high pressure as 82 MPa and why the deviation of simulation results is not as large as the deviation of stagnation density  $\rho_s$  suggests when the nozzle inlet boundary conditions  $p_{in}$ ,  $T_{in}$ ,  $\rho_{in}$ , and  $w_{in}$  instead of the stagnation quantities  $p_s$ ,  $T_s$  and  $\rho_s$  are utilized to define the jet flow in the simulations which do not take the storage tank part into consideration.
- (2) Even so, the deviation is still significant and it is always recommended that the ideal gas model should be replaced with some real gas model for high-pressure hydrogen jets. The SRK real gas model framework could be a good choice though it will remarkably increase the computational cost.
- (3) As to the Abel-Noble gas model, though its  $\rho_s$  plot performs well and is very similar to the SRK result, its deviation of inlet boundary conditions  $p_{in}$ ,  $T_{in}$ ,  $\rho_{in}$ , and  $w_{in}$  due to the real gas effect is much larger than the deviation of stagnation quantities. For a hydrogen jet with a  $p_s$  of 82 MPa and  $T_s$  of 300 K, the  $\rho_s$  has a small deviation of 2.9%. However, compared with the nozzle inlet boundary conditions based on the SRK real gas model with the Abel-Noble nozzle  $c_{in}$ ,  $w_{in}$  are the same, while  $p_{in}$  of the Abel-Noble gas model is lower by 25.46%,  $T_{in}$  is lower by 8.1%, and  $\rho_{in}$  is lower by 15.29% (comparison between the red and pink lines in Figure 5). All  $p_{in}$ ,  $T_{in}$ , and  $\rho_{in}$  tend to be smaller than the SRK ones. The Abel-Noble gas model framework expressed in Equations (21)–(24) is not so ideal to be employed in the hydrogen jet simulation when the nozzle inlet boundary

conditions  $p_{in}$ ,  $T_{in}$ ,  $\rho_{in}$ , and  $w_{in}$  are utilized.

## References

- 1) T. N. Veziroglu and F. Barbir, *Int. J. Hydrogen Energy*, 17, 391–404 (1992).
- 2) H. J. Pasman and W. J. Rogers, *J. Loss Prevent. Proc.*, 23, 697–704 (2010).
- 3) K. Mohamed and M. Paraschivoiu, *Int. J. Hydrogen Energy*, 30, 903–912 (2005).
- 4) R. W. Schefer, W. G. Houf, T. C. Williams, B. Bourne, and J. Colton, *Int. J. Hydrogen Energy*, 32, 2081–2093 (2007).
- 5) A. V. Tchouvelev, Z. Cheng, V. M. Agranat, and S. V. Zhubrin, *Int. J. Hydrogen Energy*, 32, 1409–1415 (2007).
- 6) R. Khaksarfard, M. R. Kameshki, and M. Paraschivoiu, *Shock Waves*, 20, 205–216 (2010).
- 7) R. Khaksarfard and M. Paraschivoiu, *Int. J. Hydrogen Energy*, 37, 8734–8743 (2012).
- 8) J. Kim, H. Kim, T. Setoguchi, and S. Matsuo, *J. Propul. Power*, 24, 715–721 (2008).
- 9) J. Xiao, J. R. Travis, and W. Breitung, *Int. J. Hydrogen Energy*, 36, 2545–2554 (2011).
- 10) F. Bonelli, A. Viggiano, and V. Magi, *J. Fluid Eng.*, 135, 121101 (2013).
- 11) X. Li, Q. Chen, M. Chen, Q. He, D. M. Christopher, X. Cheng, B. Chowdhury, and E. S. Hecht, *Int. J. Hydrogen Energy*, 44, 6353–6365 (2019).
- 12) D. Makarov and V. Molkov, *Int. J. Hydrogen Energy*, 38, 8068–8083 (2013).
- 13) A. Hamzehloo and P. G. Aleiferis, *Int. J. Hydrogen Energy*, 39, 21275–21296 (2014).
- 14) A. Hamzehloo and P. G. Aleiferis, *Int. J. Hydrogen Energy*, 41, 6544–6566 (2016).
- 15) N. Tsuboi, K. Fujimoto, D. Muto, M. Asahara, and A. K. Hayashi, *AIAA paper*, 2017–1232 (2017).
- 16) X. M. Tang, M. Asahara, A. K. Hayashi, and N. Tsuboi, *Int. J. Hydrogen Energy*, 42, 7120–7134 (2017).
- 17) X. M. Tang, E. Dzieminska, M. Asahara, A. K. Hayashi, and N. Tsuboi, *Int. J. Hydrogen Energy*, 43, 9094–9109 (2018).
- 18) B. J. McBride, S. Gordon, and M. A. Reno, *NASA Report*, TM-4513 (1993).
- 19) J. D. van der Waals, *Dr. Diss.*, Leiden University, The Netherlands (1873).
- 20) O. Redlich and J. N. S. Kwong, *Chem. Rev.*, 44, 233–244 (1949).
- 21) G. Soave, *Chem. Eng. Sci.*, 27, 1197–1203 (1972).
- 22) D. Y. Peng and D. B. Robinson, *Ind. Eng. Chem. Fundam.*, 15, 59–64 (1976).
- 23) N. C. Patel and A. S. Teja, *Chem. Eng. Sci.*, 37, 463–473 (1982).
- 24) K. Takeno, K. Okabayashi, A. Kouchi, N. Misaka, and K. Hashiguchi, *Int. J. Hydrogen Energy*, 42, 15426–15434 (2017).